ARTICLE

https://doi.org/10.1038/s41586-018-0431-5

Measurements of the gravitational constant using two independent methods

Qing Li[1,8], Chao Xue[2,3,8], Jian-Ping Liu[1,8], Jun-Fei Wu[1,8], Shan-Qing Yang[1]*, Cheng-Gang Shao[1]*, Li-Di Quan[4], Wen-Hai Tan[1], Liang-Cheng Tu[1,2], Qi Liu[2,3], Hao Xu[1], Lin-Xia Liu[5], Qing-Lan Wang[6], Zhong-Kun Hu[1], Ze-Bing Zhou[1], Peng-Shun Luo[1], Shu-Chao Wu[1], Vadim Milyukov[7] & Jun Luo[1,2,3]*

The Newtonian gravitational constant, *G*, is one of the most fundamental constants of nature, but we still do not have an accurate value for it. Despite two centuries of experimental effort, the value of *G* remains the least precisely known of the fundamental constants. A discrepancy of up to 0.05 per cent in recent determinations of *G* suggests that there may be undiscovered systematic errors in the various existing methods. One way to resolve this issue is to measure *G* using a number of methods that are unlikely to involve the same systematic effects. Here we report two independent determinations of *G* using torsion pendulum experiments with the time-of-swing method and the angular-acceleration-feedback method. We obtain *G* values of 6.674184×10^{-11} and 6.674484×10^{-11} cubic metres per kilogram per second squared, with relative standard uncertainties of 11.64 and 11.61 parts per million, respectively. These values have the smallest uncertainties reported until now, and both agree with the latest recommended value within two standard deviations.

A precise knowledge of *G* is not only of considerable metrological interest, but also important because of the key role of *G* in fields such as gravitation, cosmology, particle physics, geophysics and astrophysics. However, this constant is difficult to measure accurately because of the extreme weakness and non-shieldability of gravity. The first *G* value, with an uncertainty of about 1%, was obtained from Cavendish and Michell's torsion pendulum experiment[1] in 1798. Since then, more than 200 experiments have been performed to determine *G*[2,3]. However, the uncertainty of *G* has been reduced by a factor of only about 10 per century. In 2016, the Committee on Data for Science and Technology published an updated *G* value (CODATA-2014) of $6.67408(31) \times 10^{-11}$ m^3 kg^{-1} s^{-2} with a relative uncertainty of 47 parts per million (p.p.m.)[4], which is still many orders of magnitude larger than that of other important fundamental constants.

In the CODATA-2014 adjustment, fourteen values of *G* determined in the past four decades are considered with smallest relative uncertainty of 14 p.p.m. However, the difference between the largest and the smallest *G* values is close to 550 p.p.m., which is almost 40 times the magnitude of the smallest uncertainty. Up to now, no well established physical theory or mechanism has been able to explain such a wide-range scattering of the *G* value. The most probable explanation lies in undiscovered systematic errors in all or some of these experiments. In view of the different error sources in different experiments, the only way to solve this problem and improve the confidence level, as discussed by Quinn et al.[5–8], is to measure the constant using a number of different methods. At the International Bureau of Weights and Measures, Quinn and colleagues have measured *G* with two methods[9–11] and obtained results at the high end of the *G* values adopted in the CODATA-2014 adjustment. In this work, we performed a new determination of *G* using torsion pendulum experiments on different apparatus with two completely independent methods (see Supplementary Information Section 1 and Supplementary Tables 1–3)—the time-of-swing (TOS) method and the angular-acceleration-feedback (AAF) method—so that unknown systematic errors in one method would be unlikely to exist in the other.

The TOS method, most famously used by Heyl[12,13] in the 1930s, measures the change in the torsional oscillation frequency of a pendulum with the source masses arranged in two different configurations: the 'near' position, where the source masses are in line with the equilibrium position of the torsion pendulum, leading to a faster oscillation, and the 'far' position, where the source masses are perpendicular to the equilibrium position of the torsion pendulum, resulting in a slower oscillation. The AAF method was first used to measure *G* by Rose et al.[14] in 1969 and was considerably improved by Gundlach et al.[15] In this method, two turntables are used to rotate the torsion pendulum coaxially and the source masses individually. With a high-gain feedback control system, the twist angle of the fibre is reduced to about zero and thus the angular acceleration of the pendulum is equal to the gravitational angular acceleration generated by the source masses.

Experimental challenge and solution

Since the 1980s, our group has been measuring *G* with the TOS method and has obtained many phased results[16–20]. To reduce the anelastic effect (the frequency-dependent property of the torsion spring constant)[21–23] of the fibre, fused silicon dioxide (silica) fibres with high quality factor of the torsional oscillation mode (*Q*) were used in the present measurements, which were performed on two independent apparatus (Extended Data Fig. 1a–c). In the experiment using apparatus 1

[1]MOE Key Laboratory of Fundamental Physical Quantities Measurements, Hubei Key Laboratory of Gravitation and Quantum Physics, School of Physics, Huazhong University of Science and Technology, Wuhan, China. [2]TianQin Research Center for Gravitational Physics, Sun Yat-sen University, Zhuhai, China. [3]School of Physics and Astronomy, Sun Yat-sen University, Zhuhai, China. [4]College of Engineering, Huzhou University, Huzhou, China. [5]Teaching Research and Assessment Center, Henan Institute of Technology, Xinxiang, China. [6]School of Science, Hubei University of Automotive Technology, Shiyan, China. [7]Sternberg Astronomical Institute, Moscow State University, Moscow, Russia. [8]These authors contributed equally: Qing Li, Chao Xue, Jian-Ping Liu, Jun-Fei Wu. *e-mail: ysq2011@hust.edu.cn; cgshao@hust.edu.cn; junluo@hust.edu.cn

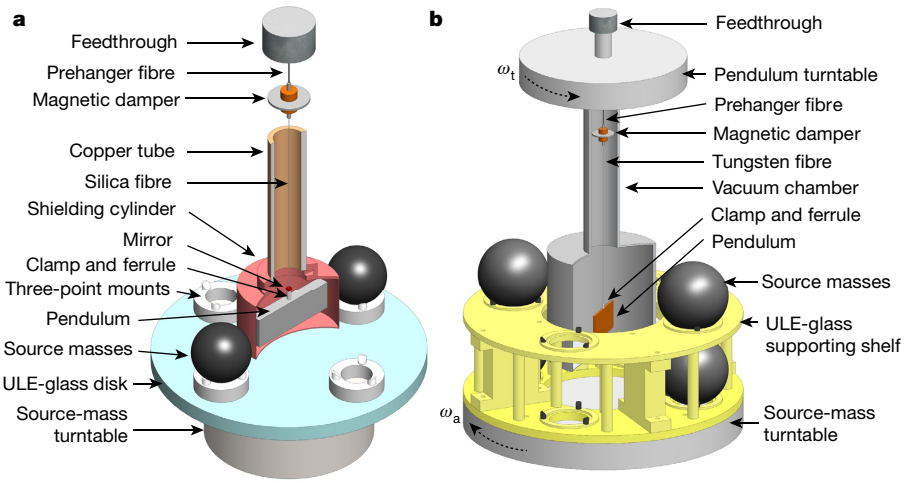

Fig. 1 | Sketch of the experiment. a, In the TOS method, the pendulum is an Al-coated fused silica block with dimensions of $91 \times 11 \times 31$ mm^3 and mass of about 68 g. The pendulum is suspended by a thin fused silica fibre with a diameter of 40–60 μm and a length of 900 mm. The magnetic damper is suspended through a 50-mm-long, 80-μm-diameter tungsten fibre. Two SS316 stainless-steel spheres with an average diameter of 57.2 mm and a vacuum mass of 778 g are used as the source masses. A turntable is used to change the positions of the spheres between the 'near' and 'far' configurations (the 'near' configuration is shown here; in the 'far' configuration, the turntable is rotated by 90°). A hollow gold-coated aluminium cylinder installed between the pendulum and the spheres is used to shield the system from the electrostatic field. The pendulum and the source masses are placed inside the same vacuum chamber with a pressure of about 10^{-5} Pa maintained by an ion pump. The pendulum twist is monitored by an optical lever. **b**, In the AAF method, the pendulum is a gold-coated fused silica block with dimensions of $91 \times 4 \times 50$ mm^3 and a vacuum mass of 40 g. The main fibre is an 870-mm-long, 25-μm-diameter tungsten fibre. The design of the magnetic damper is the same as that in the TOS method. Four SS316 stainless-steel spheres with an average diameter of 127.0 mm and a vacuum mass of 8,541 g are used as the source masses that sit on an ULE-material shelf with upper and lower layers. The small deflection angle of the pendulum is recorded by an autocollimator. The chamber with the pendulum is hung under an air-bearing turntable, which is installed coaxially with the separate source-mass turntable. The apparatus are located in the passive thermal room situated in our cave laboratory.

(TOS-I), three different silica fibres were used to check for possible fibre-induced errors while all other parts of the apparatus were unchanged for all measurements. Apparatus 2 was placed in another room, about 150 m away from apparatus 1. In the experiment with apparatus 2 (TOS-II), a new silica fibre with another set of pendulum and source masses was used to test for possible errors dependent on the apparatus. Furthermore, we minimized other large systematic uncertainties encountered in our previous experiment[18,19].

Since 2008, our group has been conducting proof-of-principle experiments with the AAF method[24,25]. In this work, the apparatus was redesigned and completely rebuilt (Extended Data Fig. 1d–f) to reduce several sources of uncertainty that existed in our previous measurements: (1) the aluminium shelf supporting the source masses was substituted with an ultra-low thermal expansion (ULE) glass shelf to reduce the influence of temperature on the distance between the source masses; (2) the turntable supporting the vacuum chamber and the pendulum was replaced by a large hollow-bowl air bearing and moved from the bottom to the top of the apparatus to improve stability; (3) two different methods were used to measure the distance between the source masses and thus improve the confidence level; and (4) the co-moving background gravity gradient created by the rotating shelf was compensated directly to reduce its effect on the G measurement. With the AAF method, we measured the G value at three different conditions (referred to as AAF-I, AAF-II and AAF-III). The selected signal frequency in AAF-I was different from the other two measurements. In AAF-III, other members of the group repeated the measurement of G with two additional improvements: the magnetic damper correction was reduced by optimizing the prehanger fibre and the magnetic effect was reduced by adding a Mu-metal shield around the pendulum.

Schematics of the two methods are shown in Fig. 1. In both methods, the heart of the apparatus is a two-stage pendulum system that consists of a magnetic damper and a torsion pendulum. The passive magnetic damper is used to suppress the swinging mode of the torsion pendulum, which is excited by ambient vibration noise[26]. Well characterized stainless-steel spheres are used as the source masses. Because the determination of G is based on Newton's formula, $F = GMm/r^2$ (where F is the gravitational force between masses M and m, which are located at a distance r), we need to measure the dimensions, density, homogeneity and relative positions of the spheres with sufficient accuracy. For this purpose, considerable efforts were devoted to grinding and polishing the pendulum block and the source masses to obtain a perfect geometry (Extended Data Tables 1, 2). The assembly and alignment of the pendulum and source masses were carried out with great care, following the method introduced in ref. [19] (Supplementary Information Section 2). To eliminate possible human errors, almost all parameters were measured repeatedly by different members of the group, and the combined uncertainties are shown in Table 1.

The silica fibre, a critical component in the TOS method, was pulled from a high-purity fused silica rod using an oxygen–natural gas flame (Extended Data Fig. 2). Four fibres with diameters of 40–60 μm, lengths of 900 mm and $Q = (2\text{–}3) \times 10^5$ were selected for the experiments to obtain an optimal signal-to-noise ratio. The fibre surfaces were sputter-coated by 5-nm-thick germanium and then 10-nm-thick bismuth to suppress the electrostatic influence from the charges accumulated on the surfaces of the pendulum and fibre. The Ge buffer layer kept the interface dissipation low, and the conductive Bi layer enabled charge flow[27]. After coating, the quality factors were decreased to $(3\text{–}6) \times 10^4$, but they were still one order of magnitude higher than that of the tungsten fibre used in our previous experiment[18,19] ($Q \approx 1.7 \times 10^3$). Considering the correction factor $1/(\pi Q)$ proposed by Kuroda[21], we estimate the correction to the G value due to anelasticity to be 5–9 p.p.m., and half of this value is treated as the uncertainty (Extended Data Table 3).

In the AAF method, precision control of the turntable rotation is a key factor. It is realized by using two feedback loops with the proportion–integration–differentiation control algorithm[25]. The angular velocity, $\omega_t(t)$, of the pendulum turntable is feedback-controlled to minimize the twist angle of the fibre to about zero (Fig. 2d). Meanwhile, the angular velocity, $\omega_a(t)$, of the source-mass turntable is controlled to maintain a constant difference (ω_d) between the angular velocities of the two turntables so that $\omega_a(t) = \omega_d + \omega_t(t)$. Both $\omega_t(t)$ and $\omega_a(t)$ vary sinusoidally and have the same amplitude. When the two feedback

Table 1 | Contributions of various experimental parameters to the main error budget of the measurements, expressed in parts per million

Parameter	TOS-I Fibre 1	TOS-I Fibre 2	TOS-I Fibre 3	TOS-II Fibre 4	AAF-I	AAF-II	AAF-III
Pendulum							
Dimensions	1.82	1.82	1.82	2.73	0.16	0.16	0.16
Attitude	0.01 [0.02]	0.01	0.05 [0.03]	0.02	0.06	0.06	0.03
Density inhomogeneity	0.20	0.20	0.20	0.20	0.46	0.46	0.46
Coating layer	0.86	0.86	0.86	0.73	0.34	0.34	0.34
Clamp and ferrule	0.15	0.15	0.15	0.33	0.70	1.05	0.48
Others	0.40	0.37	0.39	0.26	0.29	0.29	0.29
Source masses							
Masses	0.73	0.73	0.55	0.55	0.32	0.31	0.31
Horizontal distance	8.73	8.73	8.47	9.53 [9.27]	8.98	8.98	8.98
Vertical distance	–	–	–	–	5.79	5.79	5.79
Positions, alignment	1.51 [1.60]	0.64	1.81 [1.85]	0.63 [0.68]	0.57	0.62	0.35
Fibre nonlinearity	1.45	4.84	1.10 [1.03]	1.67 [1.26]	–	–	–
Fibre anelasticity	3.00	4.19	2.84	3.46	0.01	0.01	0.01
Thermal effect	0.71	3.41	0.77 [0.61]	0.97 [1.46]	0.91	0.91	0.91
Time base	0.01	0.01	0.01	0.01	0.01	0.01	0.01
Gravitational nonlinearity	0.62	0.62	0.62	0.22	–	–	–
Rotating gravity gradient	–	–	–	–	1.86	1.35	1.72
Shelf deformation	–	–	–	–	1.51	1.51	1.51
Magnetic damper	0.08	1.19	0.05	0.08	1.95	1.95	0.08
Air density	–	–	–	–	1.00	1.51	1.13
Magnetic field	2.08	2.08	2.08	0.71	3.98	3.98	0.90
Electrostatic field	0.17	0.17	0.17	0.17	–	–	–
Angle encoder	–	–	–	–	0.72	0.72	0.72
Residual twist angle	–	–	–	–	0.03	0.61	0.45
Statistical error of $\Delta\omega^2$ or α_t	10.22 [10.83]	30.67	12.03 [10.22]	13.78 [13.78]	3.44	2.60	1.34
Total	14.29 [14.74]	32.88	15.46 [14.09]	17.49 [17.35]	12.45	12.27	11.21
Combined uncertainty	13.67	32.88	13.96	15.59	–	–	–

For fibres 1, 3 and 4, each G measurement was performed twice with random orientations of the source masses. The values in the square brackets represent the values obtained in the repeated experiments. Uncertainties are one standard deviation. 'Others' includes effects due to the pendulum mass, the reflecting mirror, glues, edge flaws and the silica rod. 'Thermal effect' includes the fibre thermoelasticity in the TOS method. In the AAF method, the fibre thermoelasticity is negligible because the fibre does not twist, and the thermal effect is evaluated by modulating the temperature in the room.

loops work well cooperatively, the angular acceleration signal of the pendulum turntable of interest appears at $2\omega_d$ with an amplitude of about 462 nrad s^{-2}, and is quantified by the gravitational interaction strength between the pendulum and the spheres. This scheme helps to clearly separate the signal from the laboratory-fixed gravitational background and other similar noises in the frequency domain.

In this experiment, ω_d was usually set to a few milliradians per second so that the signal frequency ($2\omega_d$) was in a frequency (f) range with low $1/f$ noise inherent in the torsion fibre. For most of the experimental runs, $\omega_d = 5.235988(4)$ mrad s^{-1} and the signal frequency was about 1.67 mHz (uncertainties are 1σ unless stated otherwise). The average values of $\omega_t(t)$ and $\omega_a(t)$ were about 2.44 mrad s^{-1} and -2.79 mrad s^{-1} (the minus sign denotes opposite rotation direction), respectively, which were chosen to be far from the harmonic signals of the laboratory-fixed background and make the turntable operate at appropriate rotating speeds. Furthermore, when we used an angular velocity difference of $\omega_d = 7.853982(3)$ mrad s^{-1} (where $\omega_t(t) \approx 3.49$ mrad s^{-1} and $\omega_a(t) \approx -4.36$ mrad s^{-1}), the signal frequency was about 2.50 mHz in AAF-I, and we found no dependence of the result on angular velocity.

In both methods, the relative position of the spheres to the pendulum is much less critical, but the distance between the geometric centres of the spheres (Extended Data Fig. 3) must be measured with high accuracy. To improve the position stability of the spheres, updated three-point mounts were used to support the spheres. The position repeatability and the influence of temperature and vibration were investigated in detail[28]. Furthermore, a ULE-material disk or shelf was used to support the three-point mounts to reduce the temperature influence on the distance. In the TOS method, the distance of the geometric centres of the spheres was measured before and after each experiment by using the rotating gauge block method[29] with an uncertainty of less than 0.4 μm. In the AAF method, four distances (Extended Data Fig. 3) between the geometric centres of the four spheres were determined using a coordinate measuring machine with an uncertainty of less than 2.0 μm. The horizontal separations were verified with the rotating gauge block method, and the vertical surface separations were checked by inserting a small gauge block (1–2 μm thinner than the gap) in the gap between the sphere surfaces. The results obtained with different methods agree with each other within 2 μm. The temperature effect on the distances of the geometric centres of the spheres was investigated by temperature modulation experiments (Extended Data Table 4).

Main systematic errors

The analysis of systematic effects is crucial in measuring the intrinsically weak gravitational force. Some of the main systematic errors are discussed in the following (Extended Data Table 3).

Density inhomogeneity of the pendulum and source masses

In both methods, the density inhomogeneity of the pendulum body and the source masses influences the accuracy in calculating the gravitational torque and the moment of inertia of the pendulum. The planar density distribution of the glass pendulum was measured by the optical interference method[30], which provides an uncertainty of less than 0.5 p.p.m. in both methods. The density inhomogeneity of the source masses was measured using three methods: (i) scanning slices cut from the sample sphere with scanning electron microscopy[31], which yields an uncertainty of less than 0.1 p.p.m. to the value of G; (ii) measuring

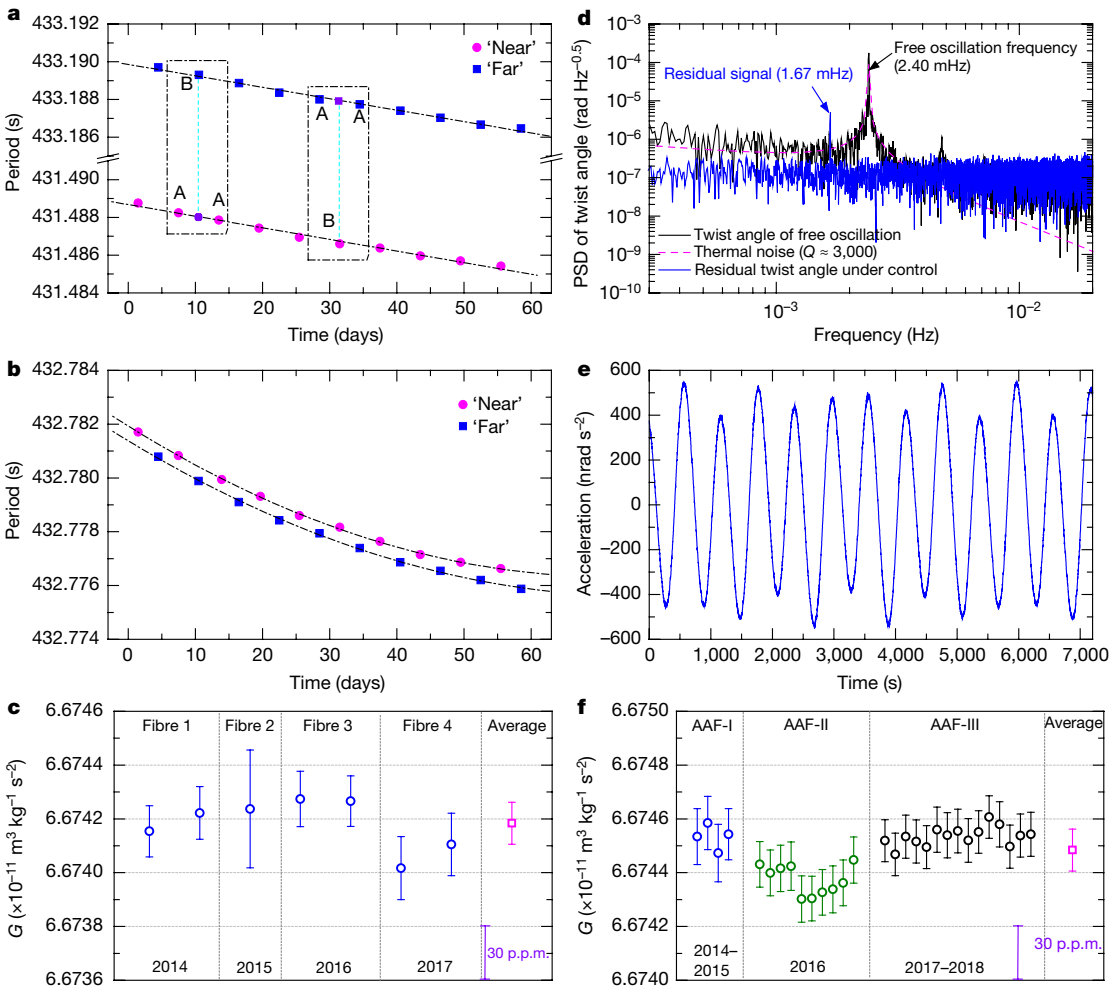

Fig. 2 | Experimental data. a, Typical periods extracted from 10 sets of time-series angle data in the TOS method for one fibre. The period difference between the 'near' and 'far' positions is about 1.7 s. The statistical uncertainty of each data point extracted from a three-day data segment is about 0.03 ms. The 'A-B-A' method[19] is used to determine the period difference and reduce the effect of the period drift (dot-dashed lines) due to the 'aging' effect of the fibre. **b**, Typical sets of background periods measured without the source masses. **c**, The 7 values of G obtained using four fibres and the TOS method. The measurement was carried out once with fibre 2 and twice with random orientations of the source masses for fibres 1, 3 and 4. **d**, The typical power spectral density (PSD) of the twist angles of the pendulum for the AAF method. At the signal frequency of interest, the typical residual twist angle of the pendulum is 17.1(3) nrad, contributing a correction of 4.37(9) p.p.m. to the value of G. **e**, Two-hour segment of the angular acceleration data of the torsion pendulum turntable. The curve is jagged mainly owing to the mixture of the laboratory-fixed environment gravitational gradient signal with the signal of interest (Supplementary Information Section 5, Supplementary Fig. 2). **f**, The values of G obtained by the AAF method. Each point denotes the value of G obtained with different orientations of the spheres. The signal frequency is about 2.50 mHz in AAF-I and ~1.67 mHz in AAF-II and AAF-III. All error bars denote 1σ confidence level.

the offset of the centre of mass from the geometric centre by using a beam balance[32]; (iii) measuring the same centre offset by using the air-bearing method. The eccentricities of the source masses determined by methods (ii) and (iii) are less than 0.3 μm in the TOS method and less than 1.3 μm in the AAF method. These eccentricities are mainly caused by nonsphericities, which were considered in the determination of the geometric centre distance between the spheres. Furthermore, the orientations of the spheres were changed randomly before each run to further average out the effects of density inhomogeneity and nonsphericity.

Magnetic damper

The magnetic damper, which is generally used to suppress the swinging modes of the torsion pendulum, introduces an additional effect to the G measurement. The correction for this effect is $I_mK^2/(IK_m^2)$ in the TOS method[19] and $I_mK/(IK_m)$ in the AAF method[24], where I and I_m are the moments of inertia of the pendulum and the magnetic damper and K and K_m are the torsion spring constants of the main fibre and the prehanger fibre, respectively. In the TOS method, we choose a ~50-mm-long, 80-μm-diameter tungsten fibre as the prehanger fibre, and a correction of only a few parts per million is required to the G value. In the AAF method, we use the same design for the magnetic damper and the prehanger fibre, which contributes a correction of 455.40(1.95) p.p.m. to the G value in AAF-I and AAF-II. This correction is reduced to 25.74(8) p.p.m. by decreasing the length (~35 mm) and increasing the diameter (150 μm) of the prehanger fibre in AAF-III (Supplementary Table 1).

Coating layer on the pendulum

The surface of the pendulum is coated with a thin metal film to eliminate the electrostatic effect. Gold is commonly used as a coating material to achieve a smooth conductive surface. The coating layer increases the moment of inertia of the pendulum and the gravitational torque exerted by the source masses. In the AAF method, a ~400-nm-thick Au/Cu layer (Cu is the sublayer) is coated on the pendulum surface, which introduces a correction of −9.10(34) p.p.m., as evaluated according to the thickness distribution and the mass of the coating layer. In a previous experiment[33] using the TOS method, the Au/Cu coating layer introduced a correction of −24.28(4.33) p.p.m. to the G value. In this work, a ~200-nm-thick aluminium layer is used to replace the Au/Cu

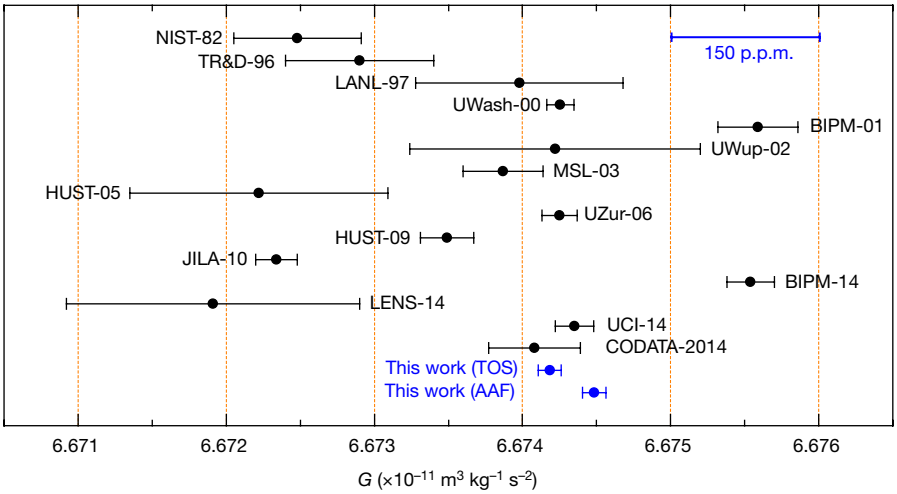

Fig. 3 | Comparison with previous results. *G* values obtained in this work compared with recent measurements (NIST-82[39], TR&D-96[40], LANL-97[41], UWash-00[15], BIPM-01[9], UWup-02[42], MSL-03[43], HUST-05[16,17], UZur-06[44], HUST-09[18,19], JILA-10[45], BIPM-14[10,11], LENS-14[47], UCI-14[46]) and the CODATA-2014 value[4]. All error bars denote 1σ confidence level.

layer, and the correction is reduced to less than 2 p.p.m. owing to the low density of Al.

Air density

In the AAF method, the source masses are located in air, outside the vacuum chamber. The volume of air displaced by the sphere introduces a negative gravitational torque at the signal frequency. The associated correction to G is ρ_{air}/ρ_{sphere}, where $\rho_{air} \approx 1.18$ kg m^{-3} is the average air density, which is monitored by an air density measurement system, and $\rho_{sphere} \approx 7{,}965$ kg m^{-3} is the average sphere density. The average correction is 148.50 p.p.m. with an uncertainty of less than 1.51 p.p.m. In each run, the correction for this effect is applied in real time according to the measured air density. In the TOS method, both the pendulum and source masses are placed in the same vacuum chamber, thus no air density effect needs to be considered.

The thermal effect

In both methods, corrections were applied for thermal effects on all the geometrical parameters, such as the pendulum's dimensions and the distance between the geometric centres of the spheres. The torsion spring constant of the fibre is also temperature-dependent owing to thermoelasticity[34]. For a small range of temperature variation, the spring constant of the fibre is linearly proportional to the temperature. The typical thermoelastic coefficient of the silica fibre used in this work was determined to be $101(1) \times 10^{-6}$ °C^{-1} using a temperature modulation experiment[23,35,36]. This coefficient is slightly different from fibre to fibre. According to the monitored temperature variation around the fibre, the correction for the thermoelastic effect was applied synchronously for each run when extracting the oscillation frequency of the pendulum in the TOS method (Extended Data Table 5).

In the AAF method, the thermoelastic effect is negligible because the fibre does not twist. In addition, the temperature variation in the room was increased to about 1 °C, and the response coefficient of angular acceleration of the pendulum turntable was measured to be $(2.2 \pm 3.6) \times 10^{-12}$ rad s^{-2} °C^{-1} (Extended Data Fig. 4). Considering that the temperature variation was less than 0.1 °C during each experimental run, it contributes an uncertainty of no more than 0.91 p.p.m.

The electrostatic effect

In the TOS method, the electrostatic disturbance was effectively reduced by the shield inserted between the pendulum and the source masses. During data acquisition, the pendulum, the shield and the source masses were all grounded. However, the fluctuation of the electrostatic potential difference between the shield and the pendulum could change the effective spring constant of the fibre and affect the oscillation period. We measured the oscillation period of the pendulum for a varying voltage applied on the shield. The typical response coefficient of the period to the voltage was −28.6(1) ms V^{-1} near 0 V, corresponding to an extra electrostatic spring constant of $1.34(1) \times 10^{-12}$ N m rad^{-1} per volt. When the spheres were exchanged between the 'near' and 'far' positions, the potential variation on the shield was measured by a digital multimeter to be less than 10 μV, which contributes an uncertainty of no more than 0.17 p.p.m. to the G value. We applied different voltages on the shield in the sequence ground, 0.1 V, −0.1 V, ground, and found that the period of the pendulum changed correspondingly, but the period differences between the 'near' and 'far' positions were consistent with each other (Extended Data Fig. 5). This further confirms that the electrostatic effect on the G measurement with the TOS method is very small.

In the AAF method, a grounded vacuum chamber made of aluminium alloy shields electrostatically the grounded pendulum from the source masses. We found no substantial influence of the pendulum oscillation on the noise spectrum when a 1-mHz square wave voltage with an amplitude of about 10 V was applied on the upper-layer spheres (Fig. 1b).

The magnetic effect

In the TOS method, the interaction between the local magnetic field and residual magnetic moment of the spheres produces an additional torque on the pendulum. The contribution of this effect to the uncertainty of G was evaluated to be 2.08 p.p.m. (in TOS-I) and 0.71 p.p.m. (in TOS-II), following the method used in ref. [37]. In the AAF method, the horizontal magnetic gradient generated by the source masses produces a periodic torque on the pendulum at a signal frequency of $2\omega_d$. We measured this correction to be 24.2(1.4) p.p.m. when an increased gradient of 0.31(1) Gs m^{-1} is produced by a current coil placed on the source-mass position. Because the background gradient induced by the four spheres is about 0.05 Gs m^{-1}, the contribution to the uncertainty of G is less than 3.98 p.p.m. in AAF-I and AAF-II. In AAF-III, three layers of Mu-metal shields were used to enclose the pendulum, and this error was reduced to less than 0.90 p.p.m.

Data acquisition and analysis

In the TOS method, all the data, including the pendulum twist, the temperature, seismic disturbances and fluctuations of the air pressure, were taken at a regular intervals of 0.5 s triggered by a rubidium clock with a stability of 1×10^{-11} (at 1 s) and a frequency accuracy $\leq 1 \times 10^{-10}$. The data taking procedure for all experimental runs was the same as that used in our previous experiments[18,19]. The acquisition time was three days for one position and the initial amplitude of the pendulum

oscillation was 3–4 mrad with an accuracy better than 56 μrad. Typically, 10 sets of data were taken with the source masses in the two configurations alternately. The periods of the pendulum oscillation at the two configurations were extracted from the time-series angle data by the correlation method[38], and a typical result is shown in Fig. 2a. The thermoelastic and nonlinear properties of the fibre and the gravitational nonlinearity of the source masses were corrected synchronously (Supplementary Information Section 3 and Supplementary Table 4). In addition, the effects of the co-moving background gravitational gradient from the turntable and the supports were measured without the source masses following the above procedure. For each fibre, 10 sets of background data were collected (Fig. 2b), which were subtracted from the result obtained with the source masses in position.

In the AAF method, all data were taken at regular intervals of 1 s triggered by the same kind of rubidium clock as that used in the TOS method. In each interval, the data obtained in the first half second (Δt) were averaged and then saved in a computer during the second half of the interval. The pendulum turntable angle was numerically differentiated twice with a time increment of $\Delta T = 10$ s to yield the angular acceleration, a typical segment of which is shown in Fig. 2e. The true amplitude of the angular acceleration is attenuated by a factor of $\sin(\omega_d\Delta t)/(\omega_d\Delta t)$ and $[\sin(\omega_d\Delta T)/(\omega_d\Delta T)]^2$ owing to the data average in the first half second and the numeric derivative, respectively (Supplementary Information Section 4). The asymmetric mass distribution and imperfection of the ULE-glass shelf and the rotating parts of the source-mass turntable can generate a gravitational signal on the pendulum at the frequency of interest. To eliminate this co-moving background gravity gradient effect, we placed specially fabricated mass blocks on the shelf to compensate for the gravity gradient, and this effect was reduced to less than 2 p.p.m. (Supplementary Information Section 5 and Supplementary Fig. 1).

In AAF-I, four data sets were recorded, each of them 3–6 days long. In each run, the orientation of each sphere was changed by a random azimuthal angle to average out the density inhomogeneity effect of the source masses. The least-squares method was used to fit the angular acceleration data of the pendulum turntable, including the signal and its harmonics, the laboratory-fixed background and its harmonics, the linear drift and the offset. In AAF-II and AAF-III, the signal frequency $2\omega_d$ was changed from ~2.50 mHz (used in AAF-I) to ~1.67 mHz. In AAF-II and AAF-III, 10 and 15 sets of data were taken with different orientations of the spheres in each run, respectively. The G values determined from the three individual experiments are consistent, as shown in Fig. 2f.

Results

The systematic and statistical uncertainties are presented in Table 1. In the TOS method, fibres 1–3 and fibre 4 were used in TOS-I and TOS-II, respectively. Because the change in the period between two positions using fibre 2 is only 10% of that obtained when using other fibres, owing to the thicker diameter of fibre 2, a larger relative uncertainty of $\Delta\omega^2$ (the change of the squared frequency of the torsion pendulum with the source masses at the two configurations) is introduced. From 2014 to 2017, the G measurement was carried out once with fibre 2 and twice with random orientations of the source masses for fibres 1, 3 and 4. We obtained seven values of G for the four fibres (Fig. 2c and Supplementary Table 2). The weighted mean values of G for fibres 1, 2, 3 and 4 are $6.674187(91)G_0$, $6.674237(219)G_0$, $6.674269(93)G_0$ and $6.674061(104)G_0$ with relative uncertainties of 13.67, 32.88, 13.96 and 15.59 p.p.m., respectively, where $G_0 = 10^{-11}$ m^3 kg^{-1} s^{-2}. These four results show good consistency within the relevant uncertainties. The correlations of the uncertainty components of the four results are discussed in Supplementary Information Section 6. Taking into account the correlation between the four fibres, the weighted mean value of G for the TOS method is $6.674184(78) \times 10^{-11}$ m^3 kg^{-1} s^{-2} with a combined relative uncertainty of 11.64 p.p.m. (1σ). The relative weights of the four G values are estimated as the reciprocal of the square of their uncertainties and are 0.345, 0.060, 0.330 and 0.265, respectively.

In the AAF method, the three experiments, AAF-I, AAF-II and AAF-III, give G values of $6.674534(83)G_0$, $6.674375(82)G_0$ and $6.674535(75)G_0$ with relative uncertainties of 12.45, 12.27 and 11.21 p.p.m., respectively (Supplementary Table 3). According to the method discussed above, the relative weights of these G values are estimated to be 0.306, 0.315 and 0.378, respectively. Taking into account the correlation between the three individual experiments (Supplementary Information Section 6), the weighted mean value of G for the AAF method is $6.674484(78) \times 10^{-11}$ m^3 kg^{-1} s^{-2} with a combined relative uncertainty of 11.61 p.p.m. (1σ).

Figure 3 shows a comparison of our results with the values of recent experiments[9–11,15–19,39–47] and the CODATA-2014 adjustment[4]. It should be emphasized that different members of our group carried out the TOS-method and AAF-method experiments on different apparatus, so there is no correlation between the systematic errors of the two methods, to the best of our knowledge. The G values obtained with the two independent methods have the smallest uncertainty reported until now and both agree with the CODATA-2014 value within a 2σ range, indicating the substantial contribution of this work to the determination of the true value of G.

Furthermore, the value obtained here with the TOS method is larger than our previous measurement (HUST-09[18,19] in Fig. 3) by more than a hundred parts per million, but we currently have no definite explanation for the inconsistency between the two results (Supplementary Information Section 7). This illustrates that determining the true value of G is very difficult, and further measurements are needed in the future.

Data availability

The data that support the findings of this study are available from the corresponding authors on reasonable request.

Online content

Any Methods, including any statements of data availability and Nature Research reporting summaries, along with any additional references and Source Data files, are available in the online version of the paper at https://doi.org/10.1038/s41586-018-0431-5.

Received: 29 April 2018; Accepted: 5 July 2018;
Published online 29 August 2018.

1. Cavendish, H. Experiments to determine the density of the Earth. *Phil. Trans. R. Soc. B* **88**, 469–526 (1798).
2. Gillies, G. T. The Newtonian gravitational constant: an index of measurements. *Metrologia* **24**, 1–56 (1987).
3. Rothleitner, C. & Schlamminger, S. Measurements of the Newtonian constant of gravitation, G. *Rev. Sci. Instrum.* **88**, 111101 (2017).
4. Mohr, P. J., Newell, D. B. & Taylor, B. N. CODATA recommended values of the fundamental physical constants: 2014. *Rev. Mod. Phys.* **88**, 035009 (2016).
5. Quinn, T. Measuring big G. *Nature* **408**, 919–921 (2000).
6. Quinn, T. Don't stop the quest to measure Big G. *Nature* **505**, 455 (2014).
7. Schlamminger, S. Fundamental constants: a cool way to measure big G. *Nature* **510**, 478–480 (2014).
8. Gibney, E. Rivals join forces to nail down Big G. *Nature* **514**, 150–151 (2014).
9. Quinn, T. J., Speake, C. C., Richman, S. J., Davis, R. S. & Picard, A. A new determination of G using two methods. *Phys. Rev. Lett.* **87**, 111101 (2001).
10. Quinn, T. J., Parks, H. V., Speake, C. C. & Davis, R. S. Improved determination of G using two methods. *Phys. Rev. Lett.* **111**, 101102 (2013).
11. Quinn, T., Speake, C., Parks, H. & Davis, R. The BIPM measurements of the Newtonian constant of gravitation, G. *Phil. Trans. R. Soc. A* **372**, 20140032 (2014).
12. Heyl, P. R. A redetermination of the constant of gravitation. *J. Res. Natl. Bur. Stand.* **5**, 1243–1290 (1930).
13. Heyl, P. R. & Chrzanowski, P. A new determination of the constant of gravitation. *J. Res. Natl. Bur. Stand.* **29**, 1–31 (1942).
14. Rose, R. D., Parker, H. M., Lowry, R. A., Kuhlthau, A. R. & Beams, J. W. Determination of the gravitational constant G. *Phys. Rev. Lett.* **23**, 655–658 (1969).
15. Gundlach, J. H. & Merkowitz, S. M. Measurement of Newton's constant using a torsion balance with angular acceleration feedback. *Phys. Rev. Lett.* **85**, 2869–2872 (2000).
16. Luo, J., Hu, Z. K., Fu, X. H., Fan, S. H. & Tang, M. X. Determination of the Newtonian gravitational constant G with a nonlinear fitting method. *Phys. Rev. D* **59**, 042001 (1998).
17. Hu, Z. K., Guo, J. Q. & Luo, J. Correction of source mass effects in the HUST-99 measurement of G. *Phys. Rev. D***71**, 127505 (2005).

18. Luo, J. et al. Determination of the Newtonian gravitational constant *G* with time-of-swing method. *Phys. Rev. Lett.* **102**, 240801 (2009).
19. Tu, L. C. et al. New determination of the gravitational constant *G* with time-of-swing method. *Phys. Rev. D* **82**, 022001 (2010).
20. Li, Q. et al. *G* measurements with time-of-swing method at HUST. *Phil. Trans. R. Soc. A* **372**, 20140141 (2014).
21. Kuroda, K. Does the time-of-swing method give a correct value of the Newtonian gravitational constant? *Phys. Rev. Lett.* **75**, 2796–2798 (1995).
22. Newman, R. D. & Bantel, M. K. On determining *G* using a cryogenic torsion pendulum. *Meas. Sci. Technol*. **10**, 445–453 (1999).
23. Yang, S. Q. et al. Direct measurement of the anelasticity of a tungsten fiber. *Phys. Rev. D* **80**, 122005 (2009).
24. Xue, C. et al. Preliminary determination of Newtonian gravitational constant with angular acceleration feedback method. *Phil. Trans. R. Soc. A* **372**, 20140031 (2014).
25. Quan, L. D. et al. Feedback control of torsion balance in measurement of gravitational constant *G* with angular acceleration method. *Rev. Sci. Instrum*. **85**, 014501 (2014).
26. Fan, X. D. et al. Coupled modes of the torsion pendulum. *Phys. Lett. A* **372**, 547–552 (2008).
27. Numata, K., Horowitz, J. & Camp, J. Coated fused silica fibers for enhanced sensitivity torsion pendulum for LISA. *Phys. Lett. A* **370**, 91–98 (2007).
28. Li, Q. et al. Research on supporting mounts of spheres in measurement of gravitational constant *G*. *Rev. Sci. Instrum*. **87**, 034504 (2016).
29. Luo, J., Wang, W. M., Hu, Z. K. & Wang, X. L. Precise determination of separation between spherical attracting masses in measuring the gravitational constant. *Chin. Phys. Lett*. **18**, 1012–1014 (2001).
30. Liu, L. X. et al. Measurement of density inhomogeneity for glass pendulum. *Chin. Phys. Lett*. **25**, 4203–4206 (2008).
31. Liu, L. X., Shao, C. G., Tu, L. C. & Luo, J. Measurement of density inhomogeneity for source masses in time-of-swing method of measuring *G*. *Chin. Phys. Lett*. **26**, 010403 (2009).
32. Guo, J. Q., Hu, Z. K., Gu, B. M. & Luo, J. Measurement of eccentricity of the centre of mass from the geometric centre of a sphere. *Chin. Phys. Lett*. **21**, 612–615 (2004).
33. Liu, L. X. et al. Precision measurement of distribution of film thickness on pendulum for experiment of *G*. *Chin. Phys. Lett*. **26**, 090402 (2009).
34. Zener, C. *Elasticity and Anelasticity of Metals* (University of Chicago Press, Chicago, 1948).
35. Luo, J., Hu, Z. K. & Hsu, H. Thermoelastic property of the torsion fiber in the gravitational experiments. *Rev. Sci. Instrum*. **71**, 1524–1528 (2000).
36. Hu, Z. K., Wang, X. L. & Luo, J. Thermoelastic correction in the torsion pendulum experiment. *Chin. Phys. Lett*. **18**, 7–9 (2001).
37. Li, Q., Liu, L. X., Tu, L. C., Shao, C. G. & Luo, J. Effect of local magnetic field in *G* measurement with time-of-swing method. *Chin. Phys. Lett*. **27**, 070401 (2010).
38. Tian, Y. L., Tu, Y. & Shao, C. G. Correlation method in period measurement of a torsion pendulum. *Rev. Sci. Instrum*. **75**, 1971–1974 (2004).
39. Luther, G. G. & Towler, W. R. Redetermination of the Newtonian gravitational constant *G*. *Phys. Rev. Lett.* **48**, 121–123 (1982).
40. Karagioz, O. & Izmailov, V. Measurement of the gravitational constant with a torsion balance. *Meas. Tech*. **39**, 979–987 (1996).
41. Bagley, C. H. & Luther, G. G. Preliminary results of a determination of the Newtonian constant of gravitation: a test of the Kuroda hypothesis. *Phys. Rev. Lett*. **78**, 3047–3050 (1997).
42. Kleinevoss, U. Bestimmung der Newtonschen Gravitationskonstanten *G*. PhD thesis (Univ. Wuppertal, 2002); http://elpub.bib.uni-wuppertal.de/servlets/DocumentServlet?id=335&lang=en.
43. Armstrong, T. R. & Fitzgerald, M. P. New measurements of *G* using the measurement standards laboratory torsion balance. *Phys. Rev. Lett.* **91**, 201101 (2003).
44. Schlamminger, S. et al. Measurement of Newton's gravitational constant. *Phys. Rev. D* **74**, 082001 (2006).
45. Parks, H. V. & Faller, J. E. Simple pendulum determination of the gravitational constant. *Phys. Rev. Lett.* **105**, 110801 (2010).
46. Newman, R., Bantel, M., Berg, E. & Cross, W. A measurement of *G* with a cryogenic torsion pendulum. *Phil. Trans. R. Soc. A* **372**, 20140025 (2014).
47. Rosi, G., Sorrentino, F., Cacciapuoti, L., Prevedelli, M. & Tino, G. M. Precision measurement of the Newtonian gravitational constant using cold atoms. *Nature* **510**, 518–521 (2014).

Acknowledgements We are grateful to R. Newman, T. Quinn, C. Speake, J. E. Faller, J. H. Gundlach, H. J. Paik, Z. H. Lu, J. Luo and S. H. Fan for discussions and suggestions. We thank Q. T. Fan, Y. T. Zhang, B. P. Wang, X. D. Fan, M. Ke, L. Zhao, Y. Tu, J. Q. Guo, D. C. Chen, W. M. Wang, X. L. Wang, X. J. Luo, X. H. Fu, J. Tang and Y. B. Cheng for their early works on *G* measurement. We thank the National Institute of Metrology (NIM) of China for the calibration of some measuring instruments, source masses and the length gauges. This work is partly supported by the National Natural Science Foundation of China under grants number 91536223, 11722542, 11325523 and 11605295, the National Basic Research Program of China under grant number 2010CB832801 and the National Precise Gravity Measurement Facility.

Reviewer information *Nature* thanks S. Schlamminger and the other anonymous reviewer(s) for their contribution to the peer review of this work.

Author contributions J.L. had the idea for the experiment. J.L. and S.-Q.Y. supervised all the experiments. Q.Li and J.-P.L. performed the experiment with the TOS method and analysed the data. C.X. and J.-F.W. performed the experiment with the AAF method and analysed the data. L.-D.Q. designed and built the feedback control system of the two turntables in the AAF method. C.-G.S. analysed all the errors and data independently. W.-H.T., H.X., L.-C.T., Q.Liu, L.-X.L., Q.-L.W., Z.-K.H., Z.-B.Z., P.-S.L., S.-C.W. and V.M. contributed to the analysis and discussion. S.-Q.Y., Q.Li and C.X. wrote the manuscript.

Competing interests The authors declare no competing interests.

Additional information

Extended data is available for this paper at https://doi.org/10.1038/s41586-018-0431-5.
Supplementary information is available for this paper at https://doi.org/10.1038/s41586-018-0431-5.
Reprints and permissions information is available at http://www.nature.com/reprints.
Correspondence and requests for materials should be addressed to S.-Q.Y., C.-G.S. and J.L.

Extended Data Fig. 1 | Photographs of the experimental apparatus. **a**, Apparatus 1, used in TOS-I. **b**, Apparatus 2, used in TOS-II. **c**, The suspended pendulum and source masses in the vacuum chamber used in the TOS method. The copper tube around the fibre is used to reduce the temperature gradient. The electrostatic shield (here elevated to show the pendulum), the three-point mounts, the ULE-glass disk and the turntable are also shown. **d**, The preliminary apparatus used to perform the proof-of-principle measurements[24,25] of G using the AAF method. **e**, The improved apparatus used in the present work. The apparatus was completely rebuilt to reduce several sources of uncertainty encountered in the proof-of-principle experiments (see text for details). **f**, The suspended pendulum and the optical path system used in the AAF method.

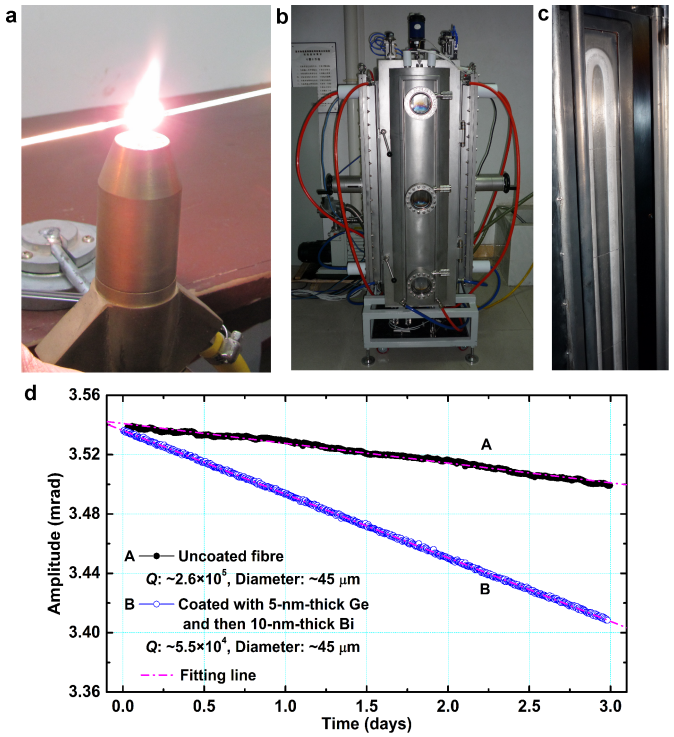

Extended Data Fig. 2 | Fabrication of the silica fibre and measurement of its *Q* factor. a, Photograph of a silica fibre pulled from a rod over an oxygen–natural gas flame. **b**, Magnetron sputtering equipment used for the coating of the silica fibres. **c**, The Bi target, with a height of ~1 m. The Ge target (not shown here) is similar. The two targets are installed on opposite sides of the coating equipment, with the fibre located between the two targets and rotated continuously. The surfaces of the fibres were coated with a 5-nm-thick Ge layer and then a 10-nm-thick Bi layer. **d**, Typical decay curves of the torsional amplitude of a pendulum suspended by a ~45-μm-diameter fibre. Curve A represents the uncoated silica fibre, with a *Q* factor of 2.6×10^5. Curve B corresponds to the coated silica fibre, with a *Q* factor of 5.5×10^4. The dot-dashed lines denote fitting curves of the exponential function $A = A_0\exp(-\pi f_0 t/Q)$, where A_0 is the initial amplitude, f_0 is the free oscillation frequency and t is the time.

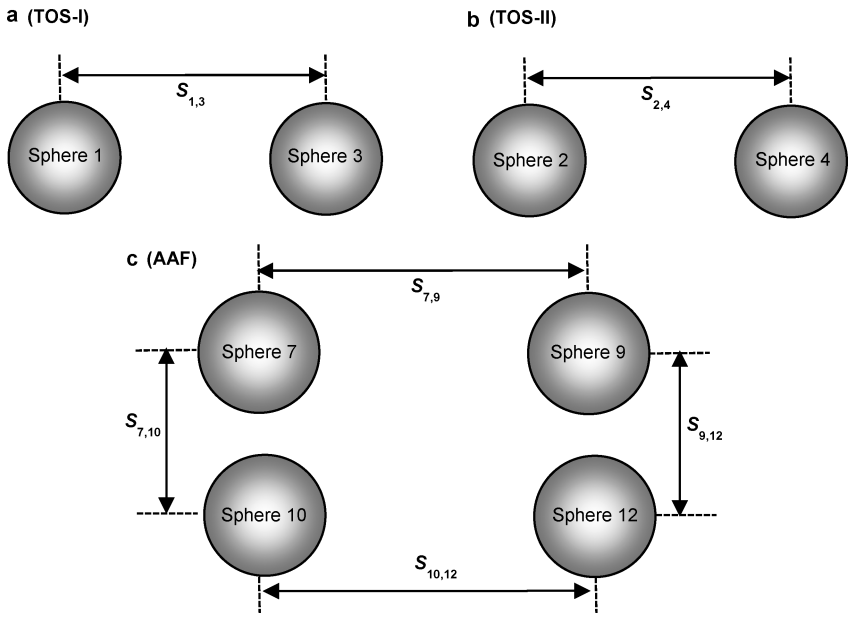

Extended Data Fig. 3 | Schematic diagram of the source masses. a, **b**, In the TOS method, spheres 1 and 3 are used in apparatus 1 (TOS-I; **a**) and spheres 2 and 4 are used in apparatus 2 (TOS-II; **b**). $S_{1,3}$ and $S_{2,4}$ are the horizontal distances of the geometric centres of the spheres in apparatus 1 and 2, respectively. **c**, In the AAF method, spheres 7, 9, 10 and 12 are used. $S_{7,9}$ and $S_{10,12}$ are the horizontal distances and $S_{7,10}$ and $S_{9,12}$ are the vertical distances between the geometric centres of the spheres.

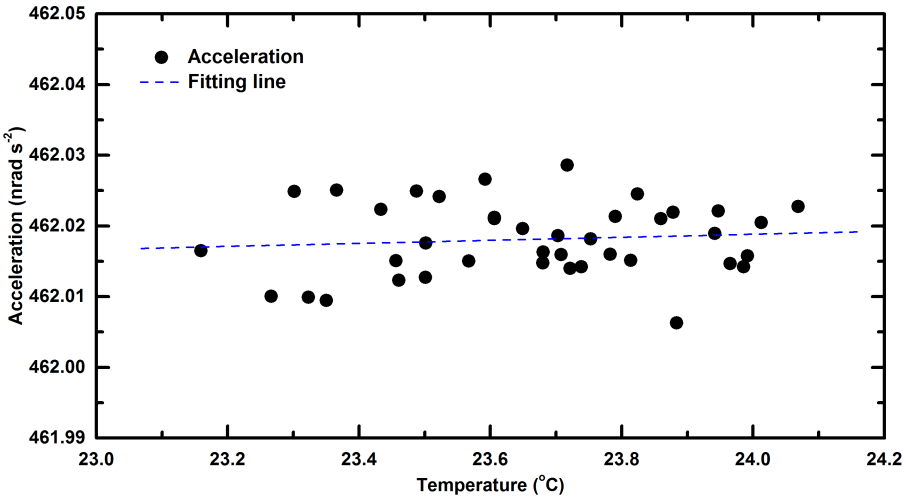

Extended Data Fig. 4 | Effect of temperature on the measurement of the angular acceleration in the AAF method. A modulation experiment was carried out by increasing the temperature variation in the room to about 1 °C. Solid circles represent the average angular acceleration of the pendulum turntable over 12-h data taking periods. The dashed line with a slope of $(2.2 \pm 3.6) \times 10^{-12}$ rad s^{-2} °C^{-1} represents the least-squares fitting curve. The result indicates that the apparatus is insensitive to the temperature variation and that a temperature variation of less than 0.1 °C during each experimental run contributes an uncertainty of less than 0.91 p.p.m. to the *G* measurement.

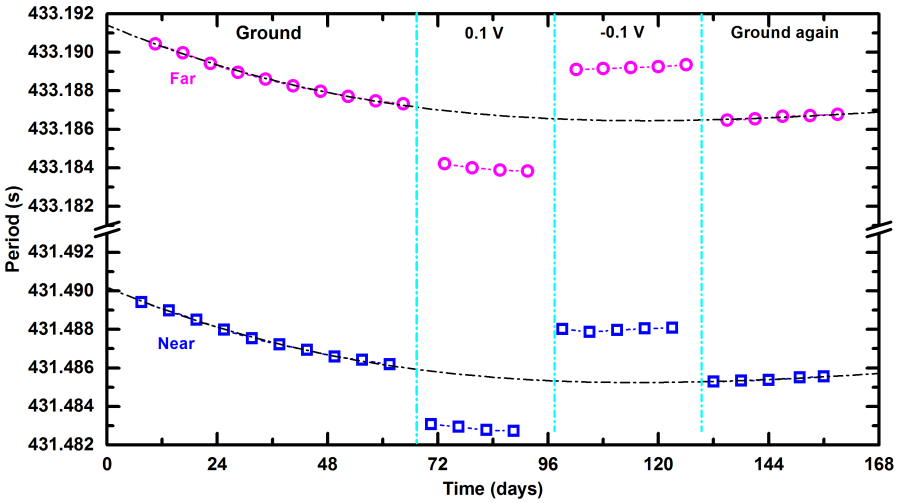

Extended Data Fig. 5 | Electrostatic effect on the measurement of the pendulum period in the TOS method. Different voltages are applied on the shield in the sequence: ground, 0.1 V, −0.1 V, ground. For each voltage, 4–5 sets of measurements of the pendulum period are performed at the 'near' and 'far' configurations. The corresponding change of the frequency squared ($\Delta\omega^2$) for the steps of the sequence is determined to be $1.662192(8) \times 10^{-6}\ s^{-2}$, $1.662184(16) \times 10^{-6}\ s^{-2}$, $1.662181(15) \times 10^{-6}\ s^{-2}$ and $1.662200(13) \times 10^{-6}\ s^{-2}$, respectively. The results show that the period changes with the applied voltage, but the $\Delta\omega^2$ values for the 'near' and 'far' configurations are consistent with each other within the statistical uncertainty. The dot-dashed lines are polynomial fitting curves that represent the period drift due to the 'aging' effect of the fibre.

Extended Data Table 1 | Dimensions and masses of the pendulums

Parameters		Length (mm)	Width (mm)	Height (mm)	Mass (g)
TOS method	Pendulum 1	91.00575(11)	11.08688(9)	30.66846(12)	68.09937(22)
	Pendulum 2	91.00336(17)	11.04448(13)	30.00446(13)	66.35715(22)
AAF method	Pendulum 3	91.05243(29)	4.00240(8)	49.92441(24)	40.0379(3)

In the TOS method, pendulum 1 is used in apparatus 1, and all the dimensions are converted to the values at 20.2 °C. Pendulum 2 is utilized in apparatus 2, and all the dimensions are converted to the values at 21.5 °C. Pendulum 3 is used in the AAF method, and all the dimensions are converted to the values at 23.7 °C. The temperature is the average value over the data acquisition period in each measurement of *G*. Uncertainties are one standard deviation.

Extended Data Table 2 | Parameters of the source masses

Parameters		Diameter (mm)	Mass (g)	Nonsphericity (μm)
TOS-I	Sphere 1	57.15072(25)	778.1630(8)	0.22(3)
	Sphere 3	57.14577(25)	777.9649(8)	0.23(3)
TOS-II	Sphere 2	57.15236(30)	778.1789(6)	0.23(3)
	Sphere 4	57.15187(31)	778.1754(6)	0.27(9)
AAF method (AAF-I, II, III)	Sphere 7	127.0003(8)	8,543.5826(53)	0.75(6)
	Sphere 9	126.9957(9)	8,541.4167(53)	0.75(6)
	Sphere 10	126.9934(8)	8,540.5282(52)	0.72(6)
	Sphere 12	126.9887(10)	8,541.5575(53)	0.89(11)

In the TOS method, spheres 1 and 3 are used in TOS-I, and all the dimensions are converted to the values at 20.2 °C. Spheres 2 and 4 are utilized in TOS-II, and all the dimensions are converted to the values at 21.5 °C. Spheres 7, 9, 10 and 12 are used in the AAF method, and all the dimensions are converted to the values at 23.7 °C. Uncertainties are one standard deviation.

Extended Data Table 3 | Comparison of several main corrections between the current experiment and our previous experiment[18,19]

Item	TOS method (in units of p.p.m.)					AAF method (in units of p.p.m.)		
	HUST-09	TOS-I: Fibre 1	TOS-I: Fibre 2	TOS-I: Fibre 3	TOS-II: Fibre 4	AAF-I	AAF-II	AAF-III
Coating layer	-24.28 (4.33)	-1.70(86)	-1.70(86)	-1.70(86)	-1.52(73)	-9.10(34)	-9.09(34)	-9.10(34)
Clamp	1,297.29 (1.62)	70.66(14)	70.65(14)	70.73(14)	68.58(33)	5.75(15)	5.85(21)	5.73(11)
Ferrule	105.22(30)	12.10(5)	12.91(5)	12.70(6)	12.85(5)	22.52(69)	22.84 (1.03)	22.45(47)
Others	11.98(21)	9.27(40)	10.19(37)	9.51(39)	8.79(26)	3.23(29)	3.29(29)	3.21(29)
Fibre anelasticity	-211.80 (18.69)	-6.01 (3.00)	-8.38 (4.19)	-5.68 (2.84)	-6.92 (3.46)	0.01	0.01	0.01
Magnetic damper	17.54(31)	0.47(8)	7.13 (1.19)	0.32(5)	0.27(8)	455.40 (1.95)	455.40 (1.95)	25.74(8)
Average Air density effect	—	—	—	—	—	149.90 (1.00)	147.33 (1.51)	148.27 (1.13)
Data averaging Δt=0.5 s	—	—	—	—	—	2.57(1)	1.14(1)	1.14(1)
Numeric derivatives ΔT=10 s	—	—	—	—	—	2,058.71 (1)	914.35(1)	914.35(1)

Coating layer**:** in the current experiment with the TOS method, the effect of the coating layer is reduced by choosing aluminium as the coating material to replace Au/Cu, which was used in a previous experiment (HUST-09)[18,19]. Clamp and ferrule: in the current experiment with the TOS method, the aluminium clamp and ferrule that used to connect the pendulum and the silica fibre in the previous experiment are miniaturized. The corresponding corrections are reduced to 1/18 and 1/8 of those in HUST-09, respectively. 'Others' includes effects due to the pendulum mass, the reflecting mirror, glues, edge flaws and the silica rod in both methods. Fibre anelasticity: this effect is reduced by choosing the high-Q silica fibre to replace the tungsten fibre used in HUST-09. Magnetic damper: this effect is reduced when the prehanger fibre is shorter and thicker. Data averaging and numerical derivatives: the true amplitude of the angular acceleration of the pendulum turntable is attenuated by a factor of $[\sin(\omega_d\Delta t)]/(\omega_d\Delta t)$ and $\{[\sin(\omega_d\Delta T)]/(\omega_d\Delta T)\}^2$ owing to averaging in the data acquisition and the use of numerical derivatives in data processing, respectively (see Supplementary Information Section 4). Values in parentheses are the uncertainties of the corrections. Uncertainties are one standard deviation.

Extended Data Table 4 | Distance between the geometric centres of the spheres

Items		Temperature (℃)	GC Distance (mm)
TOS-I: Fibre 1	First experiment	20.3	157.19245(34)
	Repeated experiment	20.3	157.19363(34)
TOS-I: Fibre 2		20.3	157.19363(34)
TOS-I: Fibre 3	First experiment	20.1	157.19392(33)
	Repeated experiment	20.1	157.19384(33)
TOS-II: Fibre 4	First experiment	21.5	157.16476(37)
	Repeated experiment	21.5	157.16489(36)
AAF method (AAF-I, II, III)	Between Sphere 7 and 9 ($S_{7,9}$)	23.7	342.2874(19)
	Between Sphere 10 and 12 ($S_{10,12}$)	23.7	342.3074(19)
	Between Sphere 7 and 10 ($S_{7,10}$)	23.7	139.7997(15)
	Between Sphere 9 and 12 ($S_{9,12}$)	23.7	139.7822(17)

In the TOS method, the temperature coefficient is measured to be less than 0.11 μm °C^{-1}. The temperature variation is less than 0.1 °C during each experimental run, which contributes an uncertainty of 0.30 p.p.m. In the AAF method, the temperature coefficient of the horizontal geometric centre (GC) distance of the upper-layer spheres is −1.9(1) μm °C^{-1}, which is used to correct the geometric centre distances. The lower horizontal and the vertical geometric centre distances are found to be constant within an uncertainty of 2 μm for a temperature change of 4 °C. Uncertainties are one standard deviation.

Extended Data Table 5 | Thermoelastic effect corrections for each fibre used in the TOS method

Items		Thermoelastic effect (in units of p.p.m.)	Average temperature (℃)
TOS-I: Fibre 1	First experiment	-73.13(0.71)	20.3
	Repeated experiment	65.08(0.71)	20.3
TOS-I: Fibre 2		723.89(3.41)	20.3
TOS-I: Fibre 3	First experiment	-146.56(0.77)	20.1
	Repeated experiment	-85.51(0.61)	20.1
TOS-II: Fibre 4	First experiment	-90.92(0.97)	21.5
	Repeated experiment	-145.59(1.46)	21.5

Uncertainties are one standard deviation.

Nature Research, brought to you courtesy of Springer Nature Limited (“Nature Research”)

Terms and Conditions

Nature Research supports a reasonable amount of sharing of content by authors, subscribers and authorised or authenticated users (“Users”), for small-scale personal, non-commercial use provided that you respect and maintain all copyright, trade and service marks and other proprietary notices. By accessing, viewing or using the nature content you agree to these terms of use (“Terms”). For these purposes, Nature Research considers academic use (by researchers and students) to be non-commercial.

These Terms are supplementary and will apply in addition to any applicable website terms and conditions, a relevant site licence or a personal subscription. These Terms will prevail over any conflict or ambiguity with regards to the terms, a site licence or a personal subscription (to the extent of the conflict or ambiguity only). By sharing, or receiving the content from a shared source, Users agree to be bound by these Terms.

We collect and use personal data to provide access to the nature content. ResearchGate may also use these personal data internally within ResearchGate and share it with Nature Research, in an anonymised way, for purposes of tracking, analysis and reporting. Nature Research will not otherwise disclose your personal data unless we have your permission as detailed in the Privacy Policy.

Users and the recipients of the nature content may not:

1. use the nature content for the purpose of providing other users with access to content on a regular or large scale basis or as a means to circumvent access control;
2. use the nature content where to do so would be considered a criminal or statutory offence in any jurisdiction, or gives rise to civil liability, or is otherwise unlawful;
3. falsely or misleadingly imply or suggest endorsement, approval , sponsorship, or association unless explicitly agreed to by either Nature Research or ResearchGate in writing;
4. use bots or other automated methods to access the nature content or redirect messages; or
5. override any security feature or exclusionary protocol.

These terms of use are reviewed regularly and may be amended at any time. We are not obligated to publish any information or content and may remove it or features or functionality at our sole discretion, at any time with or without notice. We may revoke this licence to you at any time and remove access to any copies of the shared content which have been saved.

Sharing of the nature content may not be done in order to create substitute for our own products or services or a systematic database of our content. Furthermore, we do not allow the creation of a product or service that creates revenue, royalties, rent or income from our content or its inclusion as part of a paid for service or for other commercial gain. Nature content cannot be used for inter-library loans and librarians may not upload nature content on a large scale into their, or any other, institutional repository.

To the fullest extent permitted by law Nature Research makes no warranties, representations or guarantees to Users, either express or implied with respect to the nature content and all parties disclaim and waive any implied warranties or warranties imposed by law, including merchantability or fitness for any particular purpose.

Please note that these rights do not automatically extend to content, data or other material published by Nature Research that we license from third parties.

If you intend to distribute our content to a wider audience on a regular basis or in any other manner not expressly permitted by these Terms please contact us at

onlineservice@springernature.com